# Direct growth of quasi-free-standing epitaxial graphene on nonpolar SiC surfaces

M. Ostler,[1,2] I. Deretzis,[3] S. Mammadov,[1] F. Giannazzo,[3] G. Nicotra,[3] C. Spinella,[3] Th. Seyller,[2,*] and A. La Magna[3,†]
[1]*Universität Erlangen-Nürnberg, Lehrstuhl für Technische Physik, Erwin-Rommel-Straße 1, D-91058 Erlangen, Germany*
[2]*Technische Universität Chemnitz, Institut für Physik, Reichenhainer Straße 70, D-09126 Chemnitz, Germany*
[3]*Istituto per la Microelettronica e Microsistemi (CNR-IMM), VIII strada 5, I-95121 Catania, Italy*
(Received 9 August 2012; revised manuscript received 15 July 2013; published 7 August 2013)

During the graphitization of polar SiC(0001) surfaces through thermal decomposition, a strongly bound carbon-rich layer forms at the graphene/SiC interface. This layer is responsible for the system's high electron-doping and contributes to the degradation of the electrical properties of the overlying graphene. In this study, with the aid of photoelectron spectroscopy, low-energy electron microscopy, low-energy electron diffraction, and the density functional theory, we show that if the graphitization process starts from the nonpolar $(11\bar{2}0)$ and $(1\bar{1}00)$ surfaces instead, no buffer layer is formed. We correlate this direct growth of quasi-free-standing graphene over the substrate with the inhibited formation of tetrahedral bonds between the nonpolar surface and the carbon monolayer.

DOI: 10.1103/PhysRevB.88.085408 PACS number(s): 81.05.ue, 73.22.Pr

## I. INTRODUCTION

Epitaxial graphene (EG) on SiC[1–3] is an engineered graphitic reconstruction obtained by the thermal decomposition of SiC surfaces and the subsequent Si sublimation. Commonly, EG is fabricated on production-friendly (0001) or $(000\bar{1})$ surfaces of the hexagonal polytypes 4H- and 6H-SiC.[4–6] Clean and stoichiometric $(0001)/(000\bar{1})$ surfaces are single-element terminated (referred to as Si-face or C-face, respectively) and have an in-plain lattice constant ~20% larger than that of unstrained graphene. Graphene growth on the C-face is still very challenging because it is very hard to obtain just one monolayer of EG. Thus, most applications use EG grown on the Si-face.

On the Si-face, EG is placed above an interface layer composed of carbon. This interface layer, which has a $(6\sqrt{3} \times 6\sqrt{3})R30^\circ$ periodicity with respect to the hexagonal SiC(0001) surface, is strongly bound to the substrate so that it preserves the $\sigma$ but lacks the $\pi$ bands of graphene.[7] Hence it is called the buffer layer. The buffer layer introduces donor states that effectively dope graphene.[8,9] In addition, the buffer layer is known to be detrimental for the charge carrier mobility in the graphene layers on top of it.[10] One possibility to improve the charge carrier mobility in graphene on SiC(0001) is to prepare the so-called quasi-free-standing epitaxial graphene (QFMLG) by transforming the buffer layer into graphene through the intercalation of miscellaneous elements, thereby decoupling the buffer layer from the substrate. The most promising candidate for the intercalation found so far is hydrogen.[10–12]

Although buffer layer intercalation and the subsequent formation of quasi-free-standing graphene is a promising approach, it is still unclear if this is the only process that can lead to quasi-free-standing graphene. Here, we demonstrate a method to directly grow quasi-free-standing graphene without the need of intercalation by using the low-index $(11\bar{2}0)$ and $(1\bar{1}00)$ planes as substrates.

## II. METHODS

Graphene was grown on 4H-SiC$(11\bar{2}0)$ and 4H-SiC$(1\bar{1}00)$ using sublimation growth in an Ar atmosphere.[4] The substrate material was purchased from INTRINCSIC Semiconductor. The growth was carried out in a custom build reactor described earlier.[13] Prior to growth, the samples were etched in hydrogen to remove polishing damage. The annealing time and temperature in Ar was adjusted to obtain a coverage of one to two monolayers. The samples were then investigated using x-ray photoelectron spectroscopy (XPS), angle-resolved photoelectron spectroscopy (ARPES), low-energy electron diffraction (LEED), and low-energy electron microscope (LEEM). XPS measurements are very well suited to identify a possible buffer layer[7,13] and were carried out using a SPECS PHOIBOS 150 analyzer in conjunction with a SPECS FOCUS 500 x-ray monochromator which provides monochromated Al $K_\alpha$ radiation with a photon energy of 1486.6 eV. The total energy resolution of the experiment was 0.3 eV. ARPES data was taken at BESSY II at beamline UE56/2-PGM-1 with a SPECS PHOIBOS 100 analyzer. LEEM images were used to determine the graphene layer thickness distribution. They were acquired with a SPECS FE-LEEM P90 system in our home laboratory.

To validate the experimental results we performed calculations based on the density functional theory (DFT). We studied graphene on unreconstructed and stoichiometric 4H-SiC$(11\bar{2}0)$ and $(1\bar{1}00)$ surfaces. In both cases the hexagonal symmetry of the $\{0001\}$ surfaces is absent; hence, lattice matching was achieved by building rectangular graphene/SiC supercells. The wave functions were linearly expanded on a pseudoatomic-orbital basis set. We used standard double-$\zeta$ plus polarization orbitals for Si and C, and single-$\zeta$ orbitals for the H atoms that passivate the lower termination of the slabs. Note that an extended basis set was necessary for the electronic relaxation of surfaces with a significant number of dangling bonds. The interaction between the core and valence electrons was statically described with norm-conserving pseudopotentials.[14] We employed a $2 \times 2 \times 1$ Monkhorst-Pack grid in the case of $(11\bar{2}0)$ and a $2 \times 4 \times 1$ grid in the case of $(1\bar{1}00)$ for the sampling of the rectangular Brillouin zone [Fig. 1(c)]. Real space integrals were evaluated on a mesh with a cutoff energy of 280 and 400 Ry, respectively. Atomic and supercell relaxation was achieved with a force

 ©2013 American Physical Society

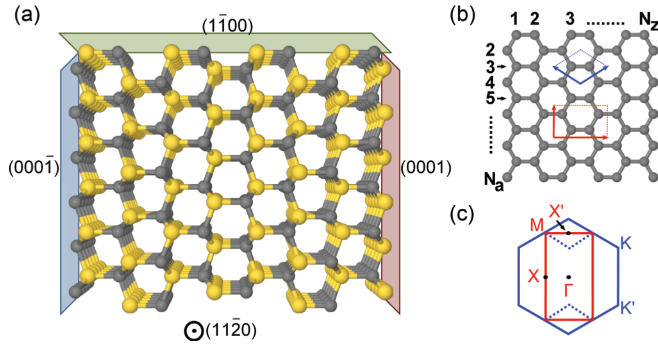


FIG. 1. (Color online) (a) Scheme of a 4H-SiC crystal, showing the low-index (0001), $(11\bar{2}0)$, and $(1\bar{1}00)$ crystallographic planes. (b) Graphene lattice, showing the hexagonal and the rectangular unit cell. A rectangular supercell can be defined on the basis of the number of its dimer lines $N_a$ and zigzag chains $N_z$. (c) Hexagonal and rectangularly folded graphene Brillouin zones.

criterion of 0.04 eV/Å. We used the SIESTA code[15] with the Perdew-Burke-Ernzerhof implementation[16] of the generalized gradient approximation (GGA) for the description of the exchange-correlation functional.

To avoid electronic alterations due to artificial strain, we geometrically identified quasicommensurate SiC/graphene heterostructures. The $SiC(11\bar{2}0)$/graphene system has surface lattice vectors parallel to the $[1\bar{1}00]$ and [0001] directions [Fig. 1(a)]. Accordingly, the total strain **s** for the graphene sheet was decomposed in two distinct uniaxial components: $\mathbf{s} = (s_{[1\bar{1}00]}, s_{[0001]})$. We found that the minimum stretching of the graphene sheet can be achieved with a supercell that has $N_a = 16$ dimer lines parallel to the $[1\bar{1}00]$ direction and $N_z = 10$ zigzag chains parallel to the [0001] direction [see Fig. 1(b)]. The resulting strain was $\mathbf{s} = (0.007, 0.013)$. The unreconstructed SiC substrate below the graphene layer consisted of five $(4 \times 2)$ $SiC(11\bar{2}0)$ layers, which were passivated by hydrogen atoms at the bottom of the slab, according to the 4H-$SiC(11\bar{2}0)$-$(1\times1)$-8H reconstruction.[17] A total of 544 atoms was included in the simulation cell. Similarly, we modeled the 4H-$SiC(1\bar{1}00)$/graphene system with a graphene supercell having $N_z = 6$ parallel to the [0001] direction and $N_a = 16$ parallel to the $[11\bar{2}0]$ direction. The substrate had a $(2 \times 4)$ periodicity with the bottom of the slab passivated by hydrogen atoms according to the 4H-$SiC(1\bar{1}00)$-$(1\times1)$-4H reconstruction.[17] In this case, the resulting strain was $\mathbf{s} = (s_{[0001]}, s_{[11\bar{2}0]}) = (0.007, -0.012)$, with the negative $s_{[11\bar{2}0]}$ value denoting a 1.2% compression of the graphene sheet. Here, a total of 384 atoms was included in the simulation cell.

## III. EXPERIMENTAL RESULTS AND DISCUSSION

Figure 2 depicts C1*s* core level spectra of graphene on (a) 4H-$SiC(11\bar{2}0)$ and (b) 4H-$SiC(1\bar{1}00)$. Additional spectra are shown of (c) quasi-free-standing monolayer graphene (QFMLG) on H-terminated 6H-SiC(0001),[12] (d) monolayer graphene (MLG) on 6H-SiC(0001),[13] and (e) the buffer layer $(6\sqrt{3})$ on 6H-SiC(0001).[13] Note that the (0001) surfaces of 6H- and 4H-SiC are identical with respect to the properties of epitaxial graphene and the interface structure. The spectra were deconvoluted into different components. For

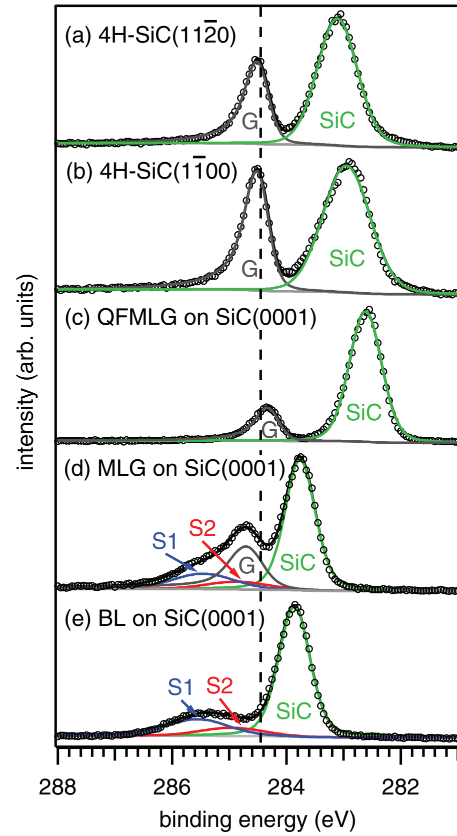


FIG. 2. (Color online) C1*s* core level spectra of (a) graphene on 4H-$SiC(11\bar{2}0)$, (b) graphene on 4H-$SiC(1\bar{1}00)$, (c) quasi-free-standing monolayer graphene on H-terminated SiC(0001), (d) monolayer graphene on SiC(0001), and (e) the buffer layer on SiC(0001). The component denoted SiC is due to the emission of C atoms in the SiC substrate. *G* marks the line is due to the graphene layer. The components *S*1 and *S*2 are characteristic for the buffer layer. All spectra are normalized to the same height of the SiC component and the curves are offset from each other for clarity. The vertical dashed line gives the C1*s* core level position of graphite.

the nonpolar surfaces the deconvolution revealed two components. The component labeled with *G* is due to the graphene layer. Its position was determined to $(284.50 \pm 0.05)$ eV for both 4H-$SiC(11\bar{2}0)$ and 4H-$SiC(1\bar{1}00)$. The other component labeled with SiC at $(283.11 \pm 0.05)$ eV for 4H-$SiC(11\bar{2}0)$ and $(282.95 \pm 0.05)$ eV for 4H-$SiC(1\bar{1}00)$ is caused by the emission from C atoms in the SiC substrate. The C1*s* spectrum of MLG on SiC(0001) shown in Fig. 2(d) is comprised of four different components.[7,13] In addition to components *G* at $(284.7 \pm 0.05)$ eV and SiC at $(283.85 \pm 0.05)$ eV there are two components *S*1 at $(285.65 \pm 0.05)$ eV and *S*2 at $(285.0 \pm 0.1)$ eV signaling the presence of the buffer layer. The same components are observed when the buffer layer is prepared on its own [see Fig. 2(e)]. On the other hand, if the buffer layer is converted into QFMLG via the intercalation of hydrogen,[11,12] the components *S*1 and *S*2 disappear. Instead, the spectrum consists of component *G* at $(284.23 \pm 0.05)$ eV and component SiC at $(282.61 \pm 0.05)$ eV. Note that the SiC component appears at different binding energies for the different samples. This is a consequence of the preparation-specific position of the surface Fermi level with respect to

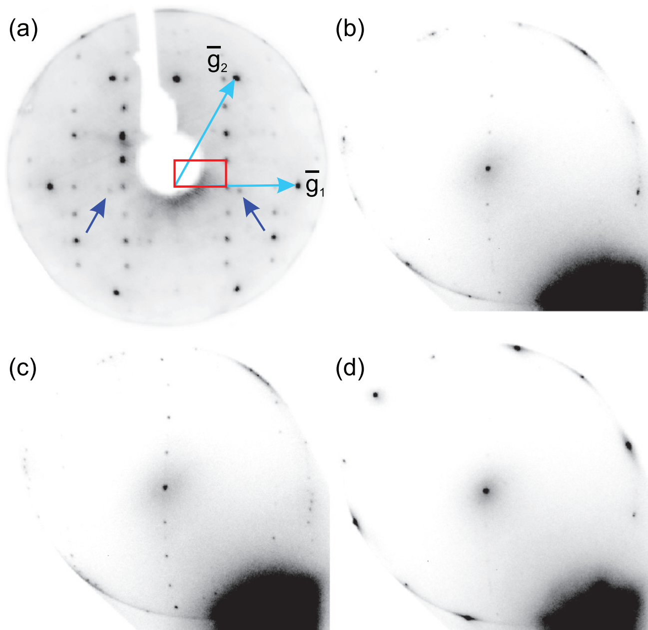


FIG. 3. (Color online) (a) Macro-LEED image of graphene on 4H-SiC(11$\bar{2}$0) taken at 140 eV and (b)–(d) $\mu$-LEED images of graphene on 4H-SiC(1$\bar{1}$00) taken at 46 eV with a 1-$\mu$m aperture at various sample positions.

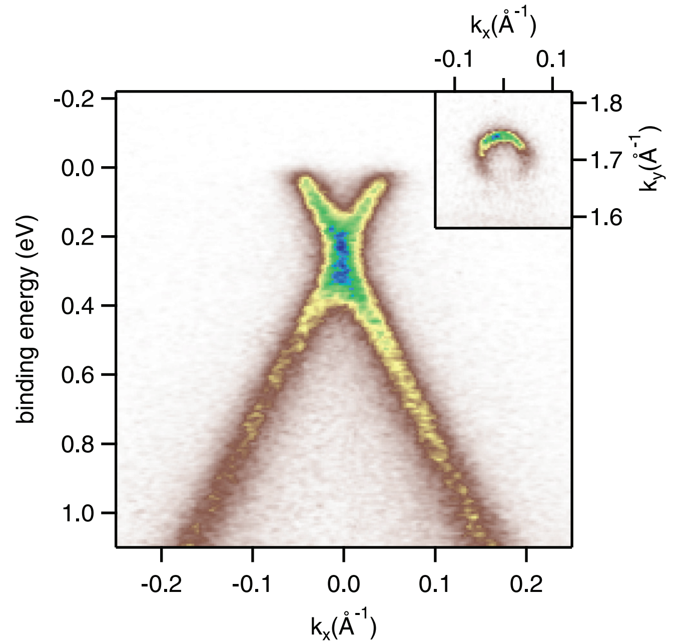


FIG. 4. (Color online) Band structure of graphene on 4H-SiC(11$\bar{2}$0) in the vicinity of the $K$-point measured in the $\overline{\mathrm{KK}}$ direction with $k_y = 1.7$ Å$^{-1}$.

the SiC band edges. The resulting variations in the surface band bending are, however, not of interest for the context of the present work. The important observation here is the lack of interface layer related components (similar to $S1$ and $S2$) in the C1$s$ spectra of the nonpolar surfaces. Apparently no strongly bound carbon layer (buffer layer) as that observed on SiC(0001) exists on these surfaces, which is in agreement with the theoretical results described below. We note in passing that a similar behavior was reported for the (000$\bar{1}$) surfaces.[7] Here, too, no buffer layer is observed. In this case, however, a $(2 \times 2)_{\mathrm{C}}$ structure has been observed[18] to exist below the graphene sheet which passivates the SiC(000$\bar{1}$) so that no strong covalent interaction is possible between the surface and the graphene sheet.[19]

A macro-LEED image of graphene on 4H-SiC(11$\bar{2}$0) is shown in Fig. 3(a). The image was acquired at an electron energy of 140 eV with the help of a regular LEED optics. The unit cell of the 4H-SiC(11$\bar{2}$0) is indicated by a rectangle. In addition to the rectangular SiC lattice, there are diffraction spots which can be described by the reciprocal lattice vectors $\vec{g}_1$ and $\vec{g}_2$ of graphene. Small arrows indicate spots that can only be explained by linear combinations of SiC and graphene base vectors. The fact that we only see six graphene spots demonstrates that there is no significant rotational disorder over the whole macro-LEED spot size in the order of mm$^2$. Of course, the small rotational disorder as was recently observed for graphene on SiC(0001) (Ref. 20) cannot be ruled out. All graphene layers are aligned so that the ΓK direction coincides with the [0001] direction of SiC [the vertical direction in Fig. 3(a)]. This is different for graphene on 4H-SiC(1$\bar{1}$00). Figures 3(b) to 3(d) show $\mu$-LEED images at 46 eV taken with a 1-$\mu$m aperture at different sample positions. In Figs. 3(b) and 3(c), one can see the SiC spots along a vertical line through the center. The distortion of the line is due to a slight misalignment of the magnetic lens system of the LEEM which was used to record the $\mu$-LEED images. At the sample position shown in Fig. 3(d), the graphene layer is too thick for the substrate to be seen at the given electron energy. The graphene spots are located at the outer edge of the LEED images. In Figs. 3(b) and 3(c) we can identify at least five graphene orientations; in Fig. 3(d) there are two. Although, we probe only about 0.8 $\mu$m$^2$ of the sample, we were not able to measure just one graphene orientation at a time indicating a high degree of rotational disorder.

With no rotational disorder, graphene on 4H-SiC(11$\bar{2}$0) qualifies as a good system for ARPES measurements. Figure 4 shows the band structure in the vicinity of the $K$ point measured at a photon energy of 65 eV. The linear $\pi$ bands cross each other 0.25 eV below the Fermi energy $E_F$. This corresponds to $n$-type doped graphene with a carrier concentration of about $4 \times 10^{12}$ cm$^{-2}$. The inset shows a circular Fermi surface with no visible states towards the Γ point. This is expected for $n$-type doped graphene.[21]

LEEM data were taken to investigate the morphology and the thickness distribution of the graphene on the nonpolar surfaces. Figure 5(a) shows a bright field image of graphene on 4H-SiC(11$\bar{2}$0) at 4.4 eV. In addition, reflectivity spectra were measured by varying the incident electron energy. Five typical spectra were observed which are presented in Fig. 5(b). The minima in the reflectivity curves are not as pronounced as they are on SiC{0001} surfaces,[22] so the unusual shape of the spectra makes it hard to assign them unambiguously to a number of layers. Nevertheless, we were able to assign the spectra to one, two, three, and four monolayers (ML) of graphene by analyzing the width of the minima structure in the spectra. Figure 5(c) depicts a false color image which was obtained by fitting the spectrum of each pixel against the

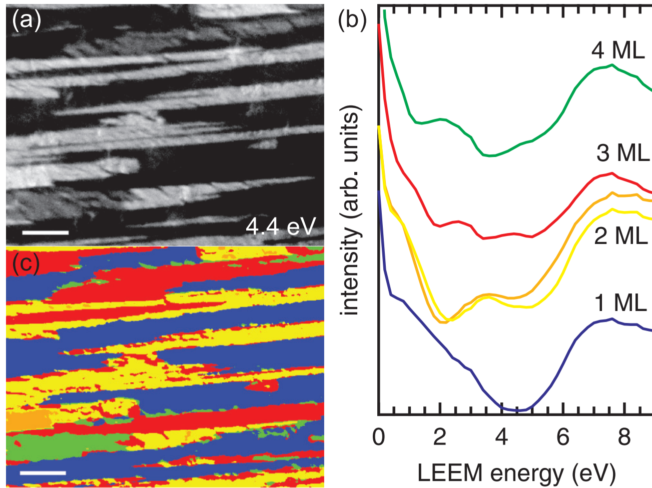


FIG. 5. (Color online) (a) LEEM bright field image at $E_{\text{LEEM}} = 4.4$ eV of graphene on 4H-SiC(11$\bar{2}$0). (b) Typical reflectivity spectra offset from each other for clarity. (c) False color image of same area as in (a) colored corresponding to the spectra shown in (b). The length of the scale bar is 1 $\mu$m.

spectra shown in Fig. 5(b). Using the false color image we calculate an average thickness of $2.0 \pm 0.1$ ML. This value is in excellent agreement with the average thickness of $2.0 \pm 0.1$ ML calculated from the intensity ratio of the surface and bulk components of the XPS C1*s* spectrum [Fig. 2(a)]. We take this as strong evidence that our assignment of the reflectivity spectra is reasonable. The false color image shows 1-$\mu$m wide terraces with continuous monolayer graphene. However, we also observe large areas of bilayer and trilayer graphene and also some areas with four ML. Similar results can be observed with graphene on 4H-SiC(1$\bar{1}$00). Figure 6(a) shows a bright field image at 2.6 eV, Fig. 6(b) shows six typical reflectivity spectra, and Fig. 6(c) shows a false color image generated in the same fashion as Fig. 5(c). Here, the minima in the reflectivity curves are more distinctive so the assignment of the spectra to one to four ML is clear. In addition, there is a flat curve [black curve in Fig. 5(b)] which can be attributed to uncovered SiC. Figure 5(c) shows that there are larger areas of monolayer, bilayer, and trilayer graphene and smaller areas of uncovered SiC and four ML graphene.

## IV. THEORETICAL RESULTS AND DISCUSSION

We start the theoretical discussion with the graphene/SiC(11$\bar{2}$0) interface. The SiC(11$\bar{2}$0) surfaces consist of parallel chains of Si and C atoms with a single dangling bond each [Fig. 7(a)]. A first-order structural analysis of the relaxed graphene/SiC(11$\bar{2}$0) heterosystem shows that the first graphene layer is flat and does not present any structural corrugation similar to the SiC(0001) buffer layer.[8] Underneath the graphene sheet, the SiC surface has structural characteristics that are similar to those of the free surface:[23–25] Si-C bond lengths are contracted by a mean of ~7% (with dimerized fluctuations typical of the 4H polytype)[25] and the Si atoms retreat towards the bulk by 0.24Å, giving rise to a mean tilt angle $\omega = 5.95^\circ$ for the surface Si-C dimers. Table I summarizes the structural parameters of the graphene/SiC(11$\bar{2}$0) interface. An immediate repercussion of Si-atom bulking is the difference in the distance between the graphene layer and the surface elements. In this sense, graphene primarily "sees" a C-type surface, although the dangling bonds of the $sp^3$configuration are not perpendicular to the graphene plane [as in the case of SiC (000$\bar{1}$)].

The rectangularly folded band structure of the system clearly shows the typical Dirac cone crossing the Fermi level, denoting the presence of undoped graphene [Fig. 7(b)]. Here, the ARPES measurements showed a small excess charge instead. However, we note that such discrepancy could simply depend on the choice of the exchange-correlation functional, which seems to be crucial for the quantitavive evaluation of the doping in epitaxial graphene systems.[26] A further

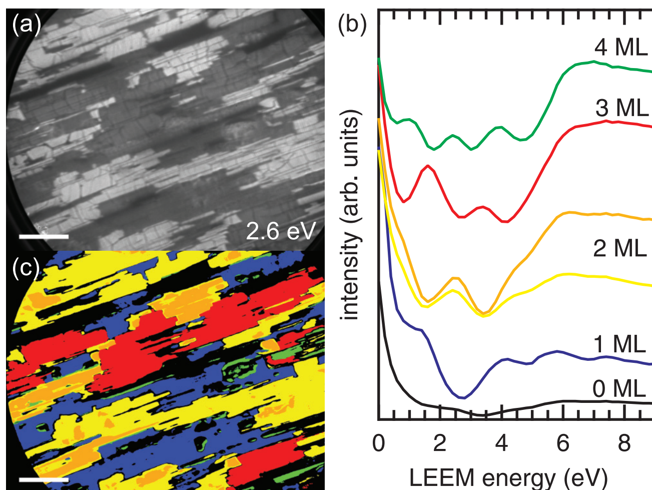


FIG. 6. (Color online) (a) LEEM bright field image at $E_{\text{LEEM}} = 2.6$ eV of graphene on 4H-SiC(1$\bar{1}$00). (b) Typical reflectivity spectra offset from each other for clarity. (c) False color image of same area as in (a) colored corresponding to the spectra shown in (b). The length of the scale bar is 1 $\mu$m.

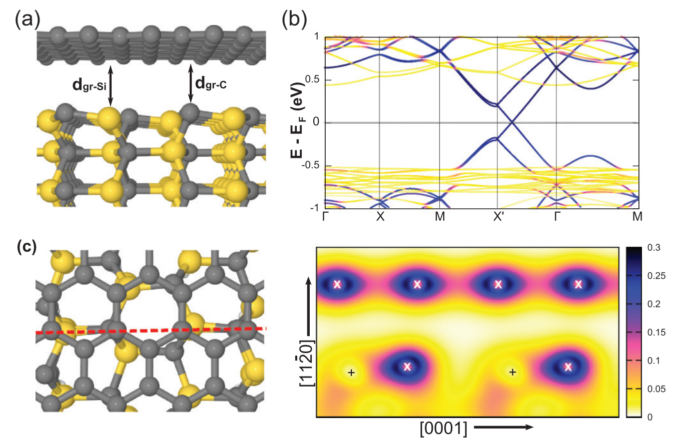


FIG. 7. (Color online) (a) Side view of the relaxed graphene/SiC(11$\bar{2}$0) interface. (b) Band structure of the graphene/SiC(11$\bar{2}$0) heterosystem, showing the contributions of the graphene (substrate) atoms as dark (bright) lines. (c) Valence charge electronic density (right) at the indicated lattice cut (left). Crosses show the positions of the interface atoms (C:×, Si:+).

TABLE I. Structural properties and binding energy for the graphene/SiC(11$\bar{2}$0) interface: minimum distance between graphene and the C surface atoms ($d_{\perp_{gr-C}}$), minimum distance between graphene and the Si surface atoms ($d_{\perp_{gr-Si}}$), tilt angle $\omega$ of the SiC(11$\bar{2}$0) surface bond, mean C-Si bond length of the the SiC(11$\bar{2}$0) surface (BL) and respective contraction with respect to the bulk value, mean C-Si bond angle centered at the C atoms of the the SiC(11$\bar{2}$0) surface ($BA_C$), mean C-Si bond angle centered at the Si atoms of the the SiC(11$\bar{2}$0) surface ($BA_{Si}$), and binding energy of graphene per atom ($E_b$).

| $d_{\perp_{gr-C}}$ (Å) | $d_{\perp_{gr-Si}}$ (Å) | $\omega$(°) | BL (Å) | $BA_C$(°) | $BA_{Si}$(°) | $E_b$ (meV) |
|---|---|---|---|---|---|---|
| 3.1 | 3.34 | 5.95 | 1.775 (−7%) | 106 | 116.8 | −10 |

band structure analysis can take place within the "fat band" representation:[8] Results show that the graphene bands are highly localized and independent from the contributions of the substrate [Fig. 7(b)]. The Dirac cone lies within the SiC band gap and overlaps with neither the half-filled nor the half-empty quasiflat bands originating from the SiC surface states.[23] The charge isocontour map [Fig. 7(c)] indicates an almost complete absence of valence charges at the interface between graphene and SiC, denoting a clear electronic detachment for the heterosystem. This aspect can be confirmed from the calculation of the binding energy $E_b$ for the graphene layer, which yields a value of 0.01 eV per graphene atom (although a small upwards correction should be considered due to the absence of van der Waals interactions in the GGA). Note that in the case of the $(6\sqrt{3} \times 6\sqrt{3})R30^\circ$-reconstructed buffer layer of the SiC(0001) surface the respective mean value is ~0.35 eV (Ref. 27) with a significant spread.

We now turn to the 4H-SiC(1$\bar{1}$00) where, contrary to 4H-SiC(11$\bar{2}$0), the minimum energy cut for the plane is not flat.[24] Surface roughness is imposed by a minimization-of-dangling-bonds criterion, which results in three-fold coordinated surface atoms with a single dangling bond each. The geometrical corrugation gives rise to a succession of (0001)- and (000$\bar{1}$)-type nanofacets that alternate parallel to the $c$ axis [Fig. 8(a)]. This topological aspect makes the study of graphene grown on SiC(1$\bar{1}$00) extremely interesting. Upon structural relaxation, also in this case there is no evidence for the formation of a strongly bound buffer layer. The graphene sheet has a mild corrugation with an amplitude of less than 0.3 Å, which follows the geometrical trend of the substrate. The SiC surface undergoes a strong relaxation, with the uppermost Si-C dimers having a bond length that is contracted by 8.4% with respect to the bulk value. Both Si and C atoms retreat towards the substrate almost equivalently, minimizing the respective tilt angle. A crucial point is that the two nanofacets are not identical, with the bond lengths in the Si facet being around 1% bigger with respect to those of the C facet, although still smaller than the bulk value (see Table II). Bulk-like features are recovered from the third substrate layer.

Electronically, graphene is decoupled from the substrate and purely $sp^2$ hybridized, as shown in the band dispersion of Fig. 8(b). Also in this case, the Dirac cone lies within the SiC band gap, although only ~0.15 eV above the half-filled bands of the surface states. The Fermi level of the system is shifted of 0.13 eV above the Dirac cone with a corresponding mild electron-doping of the order of $1.24 \times 10^{12}$ cm$^{-2}$. We notice a charge transfer from the C facet towards the Si facet. We analyze the electronic charge by means of a Bader analysis.[28] We find that a maximum charge transfer $\Delta\rho \approx 0.18\, e^-$ per Si-C dimer at the positions of the two nanofacets, which leaves an excess of holes at the C facet and an excess of electrons at the Si facet. However, due to the structural nonequivalence of the two facets, mobile charges remain also in the topmost and lowermost Si-C dimers of the surface, with the topmost dimer gaining ~0.05 $e^-$. This charge is recompensed at the lowermost dimer in order to maintain the overall neutrality. However, due to the surface roughness ($d_{\perp_{max}} - d_{\perp_{min}} = 1.4$Å), the graphene sheet "feels" the presence of negative carriers at $d_{min}$ and that of the opposing positive carriers at $d_{max}$. This spatial/charge inhomogeneity locally increases the net charge of the graphene sheet and gives rise to the soft $n$-type charging present in the system. Note that this doping mechanism is inherently different from the one present in the (0001) case, where the origin stems from interface defectiveness rather than the displacement of mobile charges.[8] Finally, the binding of the graphene sheet is stronger with respect to the (11$\bar{2}$0) case (0.058 eV per graphene atom), reflecting the presence of electrostatic interactions at the interface.

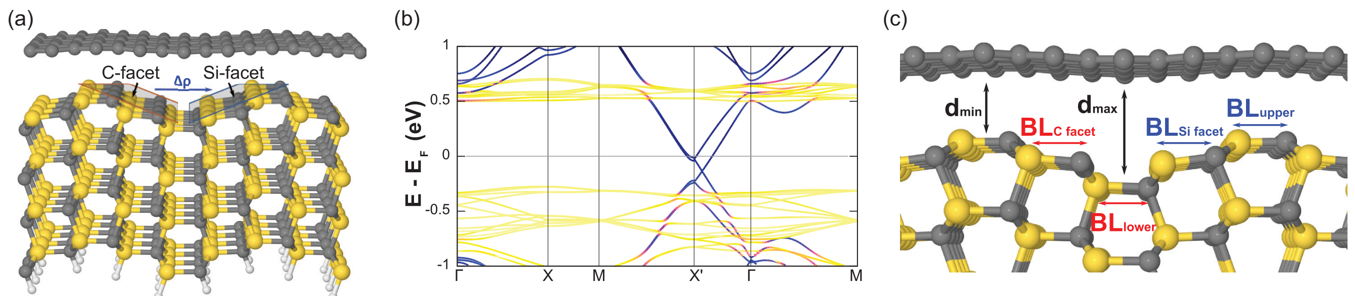


FIG. 8. (Color online) (a) Side view of the relaxed graphene/SiC(1$\bar{1}$00) interface. (b) Band structure of the graphene/SiC(1$\bar{1}$00) heterosystem, showing the contributions of the graphene (substrate) atoms as dark (bright) lines. (c) Detail of the graphene/SiC(1$\bar{1}$00) interface, indicating the structural parameters shown in Table II. The red color corresponds to Si-C surface dimers with an excess of holes whereas the blue color indicates an excess of electrons.

TABLE II. Structural properties and binding energy for the graphene/SiC($1\bar{1}00$) interface: minimum distance between graphene and the substrate ($d_{\perp_{min}}$), maximum distance between graphene and the substrate ($d_{\perp_{max}}$), C-Si bond length for the SiC($1\bar{1}00$) surface and respective contraction with respect to the bulk value [$BL_{upper}$,$BL_{lower}$, $BL_{Si-facet}$,$BL_{C-facet}$], binding energy of graphene per atom ($E_b$).

| $d_{\perp_{min}}$ (Å) | $d_{\perp_{max}}$ (Å) | $BL_{upper}$ (Å) | $BL_{lower}$ (Å) | $BL_{Si-facet}$ (Å) | $BL_{C-facet}$ (Å) | $E_b$ (meV) |
|---|---|---|---|---|---|---|
| 3.1 | 4.5 | 1.74 (−8.4%) | 1.9 (0%) | 1.89 (−0.5%) | 1.87 (−1.6%) | −58 |

Based on the previous results, it can be deduced that the driving force for the formation of the strongly bound interface layer in EG on SiC(0001) is the possibility to gain interfacial energy from the formation of tetrahedral bonds (with almost ideal bond polarity and angles) between the Si atom at the SiC surface and the C monolayer. In the case of the other SiC low index surfaces the formation of such bonds is not allowed. Weakly interacting configurations have been observed and calculated in reconstructed ($000\bar{1}$) surfaces.[18,19,29] Hence, we correlate the inhibition of tetrahedral bonds with the stability and the growth of the quasi-free-standing graphene configuration in the case of nonpolar surfaces. From an electrical viewpoint, the absence of a buffer layer should lower undesirably high doping levels and improve the overall electronic characteristics, without the need of post-annealing intercalation processes. In this sense, growth on nonpolar SiC holds great promise for epitaxial graphene use in devices and applications.

## V. CONCLUSION

In conclusion, in this work we have demonstrated with the aid of XPS, ARPES, LEEM, and DFT that quasi-free-standing graphene directly grows on the nonpolar ($11\bar{2}0$) and ($1\bar{1}00$) planes of hexagonal SiC. Both the theory and experiment confirm the absence of a buffer layer for graphene on both planes. On SiC($1\bar{1}00$), the growth resembles the one on SiC($000\bar{1}$) exhibiting large rotational disorder. The graphene layer thickness distribution is difficult to control, yielding samples with small areas of monolayer graphene and uncovered areas alongside four ML graphene. In the case of SiC ($11\bar{2}0$) we could show that graphene grows without rotational disorder, even though no buffer layer is present. The graphene coverage is more uniform with larger areas of monolayer graphene. The results could indicate alternative ways of wafer-scale graphene production based on the EG/SiC technology.

## ACKNOWLEDGMENTS

This work has been supported by the European Science Foundation (ESF) under the EUROCORES Program EuroGRAPHENE CRP GRAPHIC-RF and by the DFG in the framework of PRIORITY PPROGRAM 1459 GRAPHENE. Computations have been performed at the CINECA supercomputing facilities under project SUBGRAPH.

*thomas.seyller@physik.tu-chemnitz.de
†antonino.lamagna@imm.cnr.it

[1] C. Berger, Z. Song, T. Li, X. Li, A. Y. Ogbazghi, R. Feng, Z. Dai, A. N. Marchenkov, E. H. Conrad, P. N. First, and W. A. de Heer, J. Phys. Chem. B **108**, 19912 (2004).
[2] C. Berger, Z. Song, X. Li, X. Wu, N. Brown, C. Naud, D. Mayou, T. Li, J. Hass, A. N. Marchenkov, E. H. Conrad, P. N. First, and W. A. de Heer, Science **312**, 1191 (2006).
[3] P. N. First, W. A. de Heer, T. Seyller, C. Berger, J. A. Stroscio, and J.-S. Moon, MRS Bull. **35**, 296 (2010).
[4] K. V. Emtsev, A. Bostwick, K. Horn, J. Jobst, G. L. Kellogg, L. Ley, J. L. McChesney, T. Ohta, S. A. Reshanov, J. Röhrl, E. Rotenberg, A. K. Schmid, D. Waldmann, H. B. Weber, and T. Seyller, Nat. Mater. **8**, 203 (2009).
[5] W. A. de Heer, C. Berger, M. Ruan, M. Sprinkle, X. Li, Y. Hu, B. Zhang, J. Hankinson, and E. Conrad, Proc. Natl. Acad. Sci. USA **108**, 16900 (2011).
[6] C. Virojanadara, M. Syväjarvi, R. Yakimova, L. I. Johansson, A. A. Zakharov, and T. Balasubramanian, Phys. Rev. B **78**, 245403 (2008).
[7] K. V. Emtsev, F. Speck, T. Seyller, L. Ley, and J. D. Riley, Phys. Rev. B **77**, 155303 (2008).
[8] I. Deretzis and A. La Magna, Phys. Rev. B **84**, 235426 (2011).
[9] S. Kopylov, A. Tzalenchuk, S. Kubatkin, and V. I. Fal'ko, Appl. Phys. Lett. **97**, 112109 (2010).
[10] F. Speck, J. Jobst, F. Fromm, M. Ostler, D. Waldmann, M. Hundhausen, H. B. Weber, and T. Seyller, Appl. Phys. Lett. **99**, 122106 (2011).
[11] C. Riedl, C. Coletti, T. Iwasaki, A. A. Zakharov, and U. Starke, Phys. Rev. Lett. **103**, 246804 (2009).
[12] F. Speck, M. Ostler, J. Röhrl, J. Jobst, D. Waldmann, M. Hundhausen, L. Ley, H. B. Weber, and T. Seyller, Mater. Sci. Forum **645–648**, 629 (2010).
[13] M. Ostler, F. Speck, M. Gick, and T. Seyller, Phys. Status Solidi B **247**, 2924 (2010).
[14] N. Troullier and J. L. Martins, Phys. Rev. B **43**, 1993 (1991).
[15] J. M. Soler, E. Artacho, J. D. Gale, A. García, J. Junquera, P. Ordejón, and D. Sánchez-Portal, J. Phys.: Condens. Matter **14**, 2745 (2002).
[16] J. P. Perdew, K. Burke, and M. Ernzerhof, Phys. Rev. Lett. **77**, 3865 (1996).
[17] T. Seyller, R. Graupner, N. Sieber, K. V. Emtsev, L. Ley, A. Tadich, J. D. Riley, and R. C. G. Leckey, Phys. Rev. B **71**, 245333 (2005).
[18] F. Hiebel, P. Mallet, F. Varchon, L. Magaud, and J.-Y. Veuillen, Phys. Rev. B **78**, 153412 (2008).
[19] L. Magaud, F. Hiebel, F. Varchon, P. Mallet, and J.-Y. Veuillen, Phys. Rev. B **79**, 161405 (2009).
[20] A. L. Walter, A. Bostwick, F. Speck, M. Ostler, K. S. Kim, Y. J. Chang, L. Moreschini, D. Innocenti, T. Seyller, K. Horn, and E. Rotenberg, New J. Phys. **15**, 023019 (2013).

[21]T. Ohta, A. Bostwick, J. L. McChesney, T. Seyller, K. Horn, and E. Rotenberg, Phys. Rev. Lett. **98**, 206802 (2007).
[22]H. Hibino, H. Kageshima, F. Maeda, M. Nagase, Y. Kobayashi, and H. Yamaguchi, Phys. Rev. B **77**, 075413 (2008).
[23]G. P. Brandino, G. Cicero, B. Bonferroni, A. Ferretti, A. Calzolari, C. M. Bertoni, and A. Catellani, Phys. Rev. B **76**, 085322 (2007).
[24]E. Rauls, Z. Hajnal, P. Deák, and T. Frauenheim, Phys. Rev. B **64**, 245323 (2001).
[25]E. Rauls, J. Elsner, R. Gutierrez, and T. Frauenheim, Solid State Commun. **111**, 459 (1999).
[26]T. Jayasekera, S. Xu, K. W. Kim, and M. B. Nardelli, Phys. Rev. B **84**, 035442 (2011).
[27]G. Sclauzero and A. Pasquarello, Phys. Rev. B **85**, 161405 (2012).
[28]W. Tang, E. Sanville, and G. Henkelman, J. Phys.: Condens. Matter **21**, 084204 (2009).
[29]I. Deretzis and A. La Magna, Appl. Phys. Lett. **102**, 093101 (2013).